

# A Micromachined Electrical Field-Flow Fractionation ( $\mu$ -EFFF) System

Bruce K. Gale,\* *Student Member, IEEE*, Karin D. Caldwell, and A. Bruno Frazier, *Member, IEEE*

**Abstract**—In this work, micromachining technologies are employed to develop a miniaturized electrical field-flow fractionation (EFFF) separation system. EFFF systems are used to separate colloidal particles such as cells, liposomes, proteins, or other particulates, and to characterize emulsions and other mixtures according to particle charge density. Micromachining techniques have been used to develop existing EFFF technologies. At the present time, the limiting factor in the development of higher precision EFFF separation systems has been the manufacturing approach. In this paper, the theory behind the operation and resolution of a micron-sized EFFF ( $\mu$ -EFFF) system is described and the advantages to be gained from application of micromachining technologies are given, thus motivating the need for further miniaturization. A completely fabricated  $\mu$ -EFFF system is developed, separations are performed, and the  $\mu$ -EFFF system is compared to the theoretically predicted results as well as the results from current macro EFFF systems.

**Index Terms**— Biocompatibility, colloid, emulsions, field-flow fractionation, microchannels, microfluid flow, micromachined separation system.

## I. INTRODUCTION

A CONSTANT in the field of bioinstrumentation is the need for faster analysis with ever higher resolution. One category of analysis systems that represent a significant market is separation systems. Numerous separation methods exist for purification of both small molecules and larger complexes of molecules, such as organelles and cells. Molecular separations are usually done in high yields using ion-exchange or reverse phase chromatography which separate using chemical means, or alternatively by gel-permeation or electrophoresis, which separates samples due to differences in molecule size and charge [1]. Cells and organelles are frequently purified using centrifugation, which separates based on the buoyant mass of the cell. All of these methods have advantages in specific applications, but also have characteristic limitations. Chemical separation systems may denature proteins and electrophoresis systems often require very high field strengths. Another

type of separation system, free-flow electrophoresis, which utilizes an electric field across a curtain of buffer between two closely spaced vertical plates, is a promising alternative to the previously described separation systems. Free-flow electrophoresis allows for continuous sample injection, but requires discretization of the detection and collection systems and is limited by distortion in the fluid stream caused by the parabolic flow profile [2]. Other methods of separating molecules and cells are then needed for applications in which these limitations preclude the use of existing systems. Field-flow fractionation is the solution for some applications.

Field-flow fractionation (FFF) is a class of separation techniques that rely on a field perpendicular to the direction of separation to control the migration of particles injected into the system. Although the same types of fields are used in FFF systems as in the so-called “direct field methods,” there is no longer a requirement of complete resolution in the direction of the field, so field strengths can be lower and run times shorter. In addition to these advantages, FFF systems are elution methods and allow the collection of fractions during a separation. Since the general theory for FFF systems is well developed, the elution volumes for a given sample can be directly related to a physical parameter of the sample such as electrophoretic mobility in the case of electrical field-flow fractionation (EFFF) [1].

EFFF is a molecular separation technique first described in 1972, when its feasibility was first demonstrated using various proteins [3]. EFFF, as mentioned previously, is not a direct-field separation technique, but rather relies on an electric field perpendicular to the direction of separation (perpendicular to flow direction) to perform the separation function as shown in Fig. 1. The separations are performed in a low-viscosity liquid (typically an aqueous buffer solution) which is pumped through the separation channel. The EFFF process is based on controlling the relative velocity of injected particles by forcing them toward the wall of the channel. Particles with high electrophoretic mobility or “ $\zeta$ -potential” will pack more closely to the wall, while particles of lower  $\zeta$ -potential will form a more diffuse cloud that extends further into the flow stream, see Fig. 2. Since the flow in the channel is laminar and easily characterized i.e., parabolic, the particles will flow through the channel at particular rates based on  $\zeta$ -potential and particle size. As the particle size is easily determined using other techniques, the effect of the EFFF process is to separate particles by  $\zeta$ -potential.  $\zeta$ -potentials are thought to be involved in cellular processes, including transport through cell membranes, antigen-antibody interactions,

Manuscript received July 24, 1997; revised May 5, 1998. This work was supported by the National Science Foundation (NSF) Graduate Fellowship, Amoco Chemical Corp., and the Whitaker Foundation. *Asterisk indicates corresponding author.*

\*B. K. Gale is with the Department of Bioengineering, University of Utah, 50 S. Central Campus Drive, Rm. 2480, Salt Lake City, UT 84112 USA (e-mail: Bruce.Gale@m.cc.utah.edu).

K. D. Caldwell is with the Department of Chemistry, University of Utah, Salt Lake City, UT 84112 USA.

A. B. Frazier is with the Department of Bioengineering and the Department of Electrical Engineering, University of Utah, Salt Lake City, UT 84112 USA. Publisher Item Identifier S 0018-9294(98)08847-8.

and hormonal control.  $\zeta$ -potentials are discussed in further detail in Section II.

EFFF has all the advantages of FFF systems, i.e., the ability to perform separations on cells, large molecules, colloids, emulsions, and delicate structures such as liposomes: separations that cannot be performed by electrophoresis systems [1]. Unlike the free-flow electrophoresis systems, elution in FFF systems is zonal and proceeds through one exit port; it is, therefore, capable of significantly higher resolution of processed samples. EFFF separations can be done on particles in either the "as is" condition or following surface modification with biological molecules. Therefore, anticipated applications of EFFF systems include: cell separations, characterization of emulsions, liposomes, and other particulate vehicles for intravenous drug administration with respect to size, charge, and stability, diagnostic tests for specific molecules in colloidal suspensions, quick and accurate separations of molecules, environmental water monitoring, tests for sample contamination, and further research involving  $\zeta$ -potentials. EFFF systems also find application as sample pretreatment systems by performing an initial separation on a sample that is later collected for further testing by another analysis system.

In the last several years, great progress has been made in the fabrication of microscale separation systems. A number of successful micromachined electrophoresis systems have been created [4]–[7] as well as micromachined free-flow electrophoresis systems [8], [9]. Other liquid chromatography [10], gas chromatography [11]–[13], and hybrid [14] systems have been built using micromachining technologies. Numerous other publications show there are significant advantages to be found in micromachining separation systems including increased resolution, reduced separation times, smaller sample sizes, and increased manufacturing precision. The abilities of EFFF systems also improve dramatically when scaled into the micromachining domain.

## II. THEORY

In general, the theory behind FFF systems is well developed [15]–[18]. An understanding of the theory behind EFFF is critical in understanding the need to incorporate micromachining technology in developing improved EFFF systems.

The EFFF channel, as shown in Fig. 1, is a thin channel of rectangular cross-section with an aspect ratio (the ratio of width to thickness) over 100 (as needed to closely approximate two infinite, parallel plates [19], [20]). The flow through the channel, except in very small regions near the sidewalls, approximates flow between infinite parallel plates. Flow between parallel plates separated by small distances is laminar for the flow velocities of interest. Laminar flow is characterized by a parabolic velocity distribution which implies that the fluid velocity at the surface of the plates is zero, while it is at a maximum in the center of the channel. Thus, if a particle or group of particles were to maintain an average distance from the wall different from another particle or group of particles, their velocities through the channel would be different and they would exit the channel at distinct times.

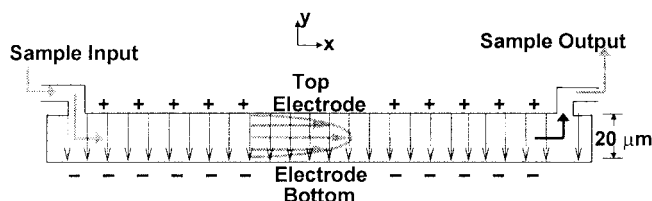


Fig. 1. Diagram of EFFF function showing parabolic flow profile, configuration of electrodes, and sample input and output ports.

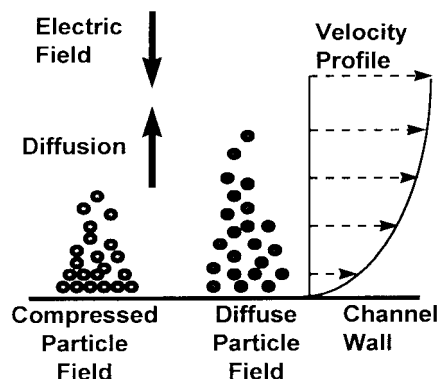


Fig. 2. Representation of forces internal to EFFF systems showing how less-compressed particle fields move ahead of more-compressed fields due to the parabolic velocity profile.

In EFFF, an electric field is used to control the average velocity of the particles in the channel by controlling the average distance that a group of particles protrudes into the flow stream with respect to the top and bottom surfaces of the microchannel. If the electric field is applied as shown in Fig. 1, particles with higher  $\zeta$ -potentials or mobilities will migrate closer to the wall of the channel than particles with lower  $\zeta$ -potential. They will protrude less into the flow stream and will, therefore, have a lower velocity than particles positioned more toward the middle of the velocity stream. This concept is quantified using (1)–(4) and demonstrated graphically in Fig. 2. The flux of particles toward the walls of the channel will be opposed by dispersive effects in the channel such as diffusion. The diffusivity,  $D$ , can be calculated using the Stokes–Einstein equation given in (1) where  $k$  is the Boltzman constant,  $T$  is the absolute temperature,  $\eta$  is the viscosity of the buffer, and  $d$  is the particle diameter. The drift velocity,  $U$ , which opposes the diffusion of the sample is given in (2) (where  $\mu$  is the electrophoretic mobility and  $E$  is the electric field strength). Therefore, at equilibrium the average thickness of the particle group will be determined by a balance between dispersive and electric forces. The ratio of  $D/U$  gives a relative measure of the thickness of this exponential particle cloud. A dimensionless number,  $\lambda$ , which corresponds to a ratio of zonal thickness to the distance between electrodes, as given in (3), can be related to the retention ratio, defined as the time required for an unretained sample to exit the system  $t_0$  divided by the time required for the particles of interest to exit  $t_e$ . This relationship is given in (4) and expresses the relationship between the tangible parameters of the system

and the physical separation [20]

$$D = \frac{kT}{3\pi\eta d} \quad (1)$$

$$U = \mu E \quad (2)$$

$$\lambda = \frac{D}{Uw} = \frac{kT}{3\pi\eta\mu dEw} \quad (3)$$

$$\frac{t_0}{t_e} = 6\lambda \left[ \coth\left(\frac{1}{2\lambda}\right) - 2\lambda \right]. \quad (4)$$

A small digression here to discuss the parameters of resolution and band broadening is in order. Both resolution and band broadening are intimately connected to the plate theory of chromatography. In plate theory, the length of a separation column can be broken down into  $N$  theoretical plates of height  $H$ . The plate height  $H$  is a measure of variance created by the separation system while the band of particles being separated moves through the channel. The total plate height can be thought of as the sum of several contributing factors. One group of factors known as instrumental factors  $H_i$  can be minimized by good instrument design and operation procedures. These factors include the structure of the instrument (wall roughness, section connections, etc.), sample plug length, and factors related to extra-column devices such as detectors and tubing. Once the instrumental factors have been minimized, the largest contributor to band broadening will be the nonequilibrium effects  $H_n$ . These nonequilibrium effects are caused by the inherent distribution of the sample over a number of volume elements and the slow movement of particles between volume elements. The plate height  $H$  is then given in (5). When the retention parameter  $R$  is increased,  $H_n$  becomes progressively smaller due to the high compaction of the bands.  $H_n$  can be found using (6) where  $\langle v \rangle$  is the average buffer velocity and  $\chi(\lambda)$  is a coefficient relating nonequilibrium plate heights to the other parameters [15].  $\chi(\lambda)$  quickly approaches  $24\lambda^3$  as retention increases [1]

$$H = H_n + H_i. \quad (5)$$

Experimentally, band broadening and plate heights  $H$  can be measured and estimates of  $H_n$  and  $H_i$  can be made by measuring the width and elution time of a sample peak for a series of flow rates [21]. Using (6) to estimate the nonequilibrium band broadening effects, a plot of plate height  $H$  versus flow velocity  $\langle v \rangle$  can be made. The intercept of this plot at zero flow velocity is the instrumental band broadening  $H_i$ , while the plate height above this value at all other flow rates is the nonequilibrium contribution  $H_n$

$$H_n = \frac{\chi(\lambda)w^2\langle v \rangle}{D}. \quad (6)$$

In EFFF systems, the instrumental band broadening is typically found by injecting acetone samples into the separation channel and measuring the plate height for a series of flow velocities. The nonequilibrium contribution to plate height  $H_n$  is found using a modified version of (6) as given in (7) [ $\chi(\lambda)$  is approximately 1/105 for acetone and other unretained samples] since the acetone is nonpolar and unaffected by the presence

of an electric field [19]

$$H_n = \frac{1}{105} \frac{w^2\langle v \rangle}{D}. \quad (7)$$

The resolution of the system,  $R_s$ , is a measure of its relative separation efficiency. The resolution can be measured experimentally by comparing the width of two particle peaks with their separation distance. For example, a resolution of one indicates two fully separated peaks. Values greater than one indicate more than full separation while values less than one indicate overlapping peaks. The resolution of a generic FFF system is given in (8) where  $S_d$  is the size selectivity index for the system,  $\Delta d$  is the difference between the diameters of the two particles, and  $L$  is the channel length [1]. For EFFF,  $S_d$  is equal to one if the drift velocity,  $U$ , is independent of particle size and the sample selectivity is only due to the differences in diffusion coefficient,  $D$  [22]. Assuming the instrumental broadening to be small or minimized and  $S_d$  equal to one, the resolution of the EFFF system  $R_s$  can be found by replacing  $H$  in (8) with the right side of (6), approximating  $\chi(\lambda)$  as  $24\lambda^3$ , replacing  $\lambda$  with a form of (3), and rearranging terms to arrive at (9), where  $V_{\text{eff}}$  is the effective voltage across the channel

$$R_s = \left( \frac{\sqrt{L}}{4} \right) \frac{\Delta d}{d} \left( \frac{S_d}{\sqrt{H}} \right) \quad (8)$$

$$R_s = \frac{(\Delta d)/(d)}{8Dw} \sqrt{\frac{L\mu^3 V_{\text{eff}}^3}{6\langle v \rangle}}. \quad (9)$$

Several important points are raised when (9) is examined closely. The resolution is inversely proportional to the separation distance of the electrodes; thus, the smaller the distance between the channel walls, the higher the resolution between two distinct particles, making EFFF an ideal application for using micromachining techniques. The resolution increases with the square root of length, so the longer the channel the better the resolution, but the time required for the improved resolution increases which is not generally desirable. The resolution depends on the effective voltage drop across the channel to the 3/2 power. Thus, increasing the applied voltage will have a positive effect on the resolution. Unfortunately, since the buffer is an aqueous solution, applied voltages above 1.7 V will provide a large enough electric field across the fluid-substrate interface to cause significant electrolysis and bubble formation. Since the EFFF system relies heavily on a stable flow system and bubbles cause serious flow abnormalities, electrolysis must be avoided. High flow velocities can limit the formation of bubbles and allow voltages above 1.7 V, but the available voltage is still small. Thus bubble formation becomes a limiting factor in determination of an appropriate applied voltage.

Another voltage related difficulty is in calculating or even measuring the effective field in the channel. Even though the applied voltage is easily measured and the applied field is equivalent to the applied voltage divided by the electrode separation distance  $w$ , the resulting effective electric field will not be constant in the channel due to the effects of ionic particle build up at the electrode—buffer interface. The double layer of ions that builds up at the interface will cause

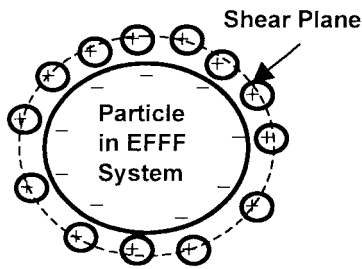


Fig. 3. Diagram of double-layer formation around charged particles in aqueous solution creating a  $\zeta$ -potential due to the shear plane.

most of the voltage drop to occur very close to the channel walls and will shield most of the channel from the applied voltage. Therefore, the effective field available to perform the separation function of the EFFF system is greatly reduced. Previously reported data [22] and results from our own lab indicate that the effective field across the channel is in the range of 0.25%–1% of the applied field depending on the composition of the buffer. Though this double-layer effect greatly reduces the capabilities of the EFFF system, the system still has proven to be effective in performing separations quickly.

$\zeta$ -potentials are another ion double-layer effect. Charged particles in the buffer solution will attract ions of opposite charge as shown in Fig. 3. The ions will shield the particle from the field to some extent as mentioned previously. These shields will also cause the particle to “appear” larger than it is in reality. In effect, a shear plane is created at some distance from the particle. The location of this shear plane will vary with the charge of the particle and the concentration of ions in the buffer solution. The  $\zeta$ -potential is the effective charge of the particle at this shear plane and is related to the volume enclosed by the shear plane [23], [24]. This  $\zeta$ -potential is the factor that determines the behavior of the particle when it is placed in an EFFF system.

The establishment of equilibrium in the channel is not instantaneous and requires a relaxation time  $\tau$  equal to the time required for a particle to migrate from one electrode to the other in the presence of the applied electric potential. If the drift velocity  $U$  is constant, the relaxation time will be found using (10). In the  $\mu$ -EFFF systems, the relaxation time typically is less than 3 s, but in larger EFFF systems may be over 5 min

$$\tau = \frac{w^2}{\mu V_{\text{eff}}} \quad (10)$$

One concern that arises when examining the mechanism of separation in EFFF systems is the fact that it is the parabolic flow profile that performs the separation function. Indeed, particles with equal and opposite  $\zeta$ -potential will elute at the same time from the channel. This can be a problem in samples containing both positively and negatively charged particles. Most samples, though, and especially biological samples, are of a uniform charge type. Biological samples contain primarily negatively charged particles (at least the particles of interest) and so any possibly ambiguous results are minimized.

The parabolic flow profile might also be expected to exist in the transverse direction of the channel. A parabolic distribution in this direction would serve to increase band broadening and reduce the resolution of EFFF systems. Thus a high aspect-ratio channel is required to remove this effect. Past results indicate that aspect ratios over 100 closely approximate two infinite parallel plates, effectively eliminating this transverse parabolic flow profile [19]. There is only a slight disruption of this approximation at the edges. The infinite parallel plate approximation can be improved by increasing the aspect ratio and optimizing the edge surface using precise manufacturing processes. Micromachining is ideal for both increasing the aspect ratio and creating precise, smooth sidewalls.

Another fluid-flow-related concern with the  $\mu$ -EFFF system is the predictability of fluid-flow parameters at the small dimensions found in the  $\mu$ -EFFF system. Much research has been conducted recently in the area of microfluidics to indicate that macro-scale flow theory is generally applicable in the micro domain, at least in terms of flow profiles [25], [26]. Thus, potential unrecognized scaling considerations are likely to have little impact on the operation of the  $\mu$ -EFFF system, though a recognition that different dynamic forces dominate at low Reynolds' numbers is required.

A related concern that can be of critical importance in  $\mu$ -EFFF systems is Joule heating of the buffer due to the applied electric field. Temperature is an important parameter in EFFF systems and significant heating can corrupt the results, especially if the heating is not consistent and uniform. Generally it is best to minimize the heating of the buffer. The amount of heat generated is directly related to the power input. Assuming a uniform field and a constant current, the heat-generated  $Q$  is the product of the power and the amount of time the buffer is in the field and can be derived from basic equations as shown in (11), where  $\alpha$  is the aspect ratio,  $V$  is the applied voltage, and  $\rho_e$  is the electrical resistivity of the buffer. Assuming all the heat generated is held in the buffer and not transferred to the surrounding materials, the change in temperature of the buffer can be found using (12), where  $C_p$  is the specific heat capacity,  $\Delta T$  is the temperature change, and  $\rho_m$  is the density of the buffer. The temperature change of the buffer can be found by inserting (11) into (12) with (13) as the result

$$Q = \frac{\alpha V^2 L^2}{\rho_e \langle v \rangle} \quad (11)$$

$$\Delta T = \frac{Q}{C_p \rho_m \alpha w^2 L} \quad (12)$$

$$\Delta T = \frac{V^2 L}{C_p \rho_m w^2 \rho_e \langle v \rangle} \quad (13)$$

The predicted temperature change found from these equations is well below any point of concern. With typical voltages of 1.5 V and using the physical parameters of water ( $\rho_m = 1000 \text{ kg/m}^3$ ,  $C_p = 4.2 \text{ kJ/kg-K}$ ) which is the principal constituent of most buffer solutions, the expected temperature change can easily be calculated. Using a 20- $\mu\text{M}$   $\text{NH}_4\text{HCO}_3$  buffer solution as an example with an empirically measured resistivity,  $\rho_e$  of 110  $\text{k}\Omega\text{-m}$ , a very slow flow velocity of

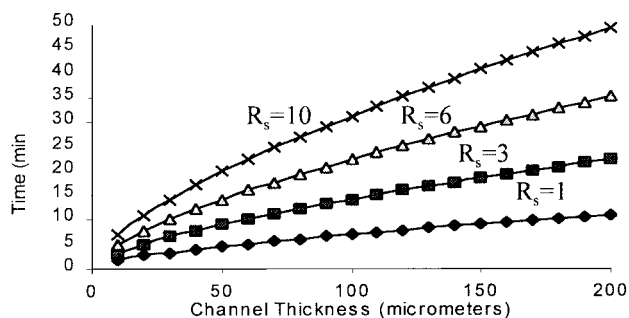


Fig. 4. Theoretical representation of the separation time for 44- and 63-nm particles at discrete values of resolution and channel thickness.

0.01 cm/s, a channel 6-cm long, 20  $\mu\text{m}$  in height, and (13) to calculate the temperature change in the channel, the temperature change is much less than 1 K (0.73 K), which has almost no effect on the EFFF system and is much less than typical room-temperature variations. Thus, Joule heating is not expected to be a significant problem in  $\mu$ -EFFF system, especially when we remember this calculation makes the conservative assumption that no heat transfer occurs between the buffer and its surroundings.

Application of micromachining technologies (i.e., an isotropic etching of silicon in potassium hydroxide (KOH), thick polyimide micromolding, wafer to wafer bonding) will allow for great improvements to be made in EFFF systems. By using (10) as the model for the resolution of an EFFF system, several distinct advantages become apparent when micromachining technologies are used to produce an EFFF system. For example, separating 127- and 252-nm polystyrene spheres in a 6-cm  $\mu$ -EFFF system with channel height of 20  $\mu\text{m}$  and a flow rate of 0.25 cm/s would yield a resolution of 5.8 and a run time of about 5 min. (A resolution of one indicates complete separation of the two populations.) To equal the same resolution using the current EFFF technology with the same applied voltage (with a channel thickness of 178  $\mu\text{m}$ , a channel width of 2 cm, and a length of 64 cm) would require a run of 390 min or 6.5 h—nearly two orders of magnitude larger! All  $\mu$ -EFFF runs could be performed using much smaller sample sizes (0.1  $\mu\text{L}$  compared to 5  $\mu\text{L}$ ). Several additional advantages for the micromachined system are found when compared with the macroscopic system including: reduced system costs, ease of batch fabrication, disposability, opportunity for systems with multiple separation channels for parallel processing, and the possibility of integrating sensors and circuitry for a “smart” micro EFFF system.

Fig. 4 is a graphical representation of (9) and shows the separation time drops at a given resolution as the channel thickness decreases. Model results have been confirmed in testing of the fabricated  $\mu$ -EFFF system.

### III. MATERIALS AND BIOCOMPATIBILITY CONSIDERATIONS

If the  $\mu$ -EFFF system is to be implemented in testing biological fluids, materials will need to be used that are both biocompatible and micromachinable. Silicon, the main component of most micromachining systems is known to be reasonably biocompatible [27], but should not contact

the biological material passing through the channels in any consequential way. Only the channel surfaces will come in contact with the fluid in the channels, so they are the materials that will need to be proven biocompatible. The materials used to make up the channels in the  $\mu$ -EFFF system are photosensitive polyimide, titanium, and gold. The titanium and gold will be used to form the top and bottom portions of the channel and will also serve as electrodes. The polyimide will be used to form the sidewalls of the channel. All of these materials fit in nicely with the technologies associated with micromachining.

1) *Photosensitive Polyimides*: Photosensitive polyimides have been used by the microelectronics industry for over a decade now and have proven to be very useful materials because of their low dielectric constant, excellent mechanical properties, high thermal stability, low water absorption, and lithographic sensitivity. The main uses of photosensitive polyimides include service as a dielectric or insulator, as a material for encapsulation of microelectronic components [28], micromolds [29], and many others. Considering that polyimides are already a major component of microelectronic devices, polyimides would be an ideal material to use as an encapsulant or to serve as channel walls if they were biocompatible. Photosensitive polyimides would prove even more valuable since precise dimensional control can be achieved by use of photolithographic techniques. Initial biocompatibility testing of polyimides is positive to date and indications are that it will serve nicely as a material in the  $\mu$ -EFFF system [30]–[34]. Note that in the EFFF system, only physical separation of biomaterials is required. There are no chemical reactions occurring that could be affected by the channel materials such as would be a concern in a micro polymerase chain reaction (PCR) system.

Since photosensitive polyimides appear ideal for use in the EFFF system, the main question to answer is how biocompatible is the material. Unfortunately, none of the previously referenced studies dealt specifically with photosensitive polyimides. Photosensitive polyimides have unique characteristics such as an added photoreactive agent which starts the polymerization reaction. These photoreactive groups are not released until a final cure is done at high temperatures. Unfortunately, during the high-temperature cure loss of water, solvent, and the leaving group (containing the photoreactive component) cause the polyimide to shrink by as much as 40% making prediction of the final material dimensions difficult [28]. Problems with sidewall profiles and film stresses can also arise as the polyimide cures. However, the large aspect ratios in the  $\mu$ -EFFF systems are designed to minimize edge effects so the shrinking is not a problem. One biocompatibility concern is the large amount of the material existing as small molecules (i.e., unreacted monomer, solvent, leaving groups) among the much larger polymer matrix. Outgassing of solvents and other small molecules are known to cause biocompatibility problems. The best way around this problem is to cure the polyimide at a high temperature for a long period of time to force any small particles out of the polymer matrix. A long enough cure should allow the photosensitive polyimide to mimic normal polyimides in terms of biocompatibility.

Another potential problem with polyimide is swelling due to water absorption. The polyimide channels as envisioned in the  $\mu$ -EFFF system will be in direct contact with the buffer solution which in most cases is an aqueous solution. Since the channel thickness  $w$  is such a critical parameter in the EFFF system, any slight swelling could cause significant trouble in collecting and interpreting data. Measurements in this area will need to be made to ensure the swelling is either minimized or well characterized.

2) *Titanium and Gold:* Gold and Titanium will be used as the electrodes of the micromachined EFFF system and will, therefore, serve as the top and bottom of the EFFF channel. Gold will be used for several reasons including its excellent electrical properties, superb corrosion resistance, and high biocompatibility. Electrically, gold is almost ideal. Electrodes formed with gold yield consistent electric fields and have extremely low resistivity [35], [36]. Gold's intrinsic corrosion resistance helps make it a highly biocompatible material and ideal for our application in which the gold will be in close proximity to salt solutions and biological materials. Titanium is necessary since the gold does not adhere well to silicon, but does adhere well to titanium. Titanium is similar to gold in that it is highly biocompatible and is used regularly as an implant material [35], [36].

3) *Preliminary Biocompatibility Testing:* Since separations of cells and cellular components is of general interest in FFF systems [37], hemolysis testing was performed using the  $\mu$ -EFFF devices, the photosensitive polyimide, and the silicone used in the interface design. This testing involved placing 2 g of crushed  $\mu$ -EFFF devices [about one-half of a 3-in (76-mm) wafer] into a test tube with 10-mL of PBS (8.5 g NaCl + 0.2 g NaH<sub>2</sub>PO<sub>4</sub>H<sub>2</sub>O + 0.47 g Na<sub>2</sub>HPO<sub>4</sub> [anhydrous] in 1-L H<sub>2</sub>O, adjusted to pH 7.4 with NaOH). Two-gram samples of cured polyimide and silicone rubber were also run separately to determine if there was any hemolysis caused by these materials in a higher concentration. A positive (detergent) and negative (glass) control were also prepared in a similar manner.

The sheep blood samples were prepared by placing 0.5 mL of blood in a 5-mL test tube and adding PBS until the tube was about one-third full. A blood sample for each test was prepared in this manner. Each sample was centrifuged three times at low speed until the cells were separated. The supernatant was drawn off after each spin down with additional PBS being added between each spin down to wash the cells. After the final run in the centrifuge, 0.2 mL of blood cells were taken and added to each of the material samples prepared earlier.

Each of the mixtures was then incubated in a water bath at 37 °C for 1 h. The supernatant was then drawn from each sample and 5 mL test tubes were filled about three-quarters full. The supernatant was then centrifuged at high speed for about 5 min or until the blood cell bodies were completely removed. The amount of absorbance at 520 nm for each sample was then measured using the spectrophotometer that was zeroed using a blank (PBS in test tube). The percent hemolysis for each sample was then calculated by dividing the difference between the test sample and the negative control by the difference between the positive control and the negative control.

#### IV. EXPERIMENTAL

Current macro scale EFFF systems are constructed using two slab conductors with a thin, patterned mylar sheet between them [22]. The mylar acts as a dielectric spacer and defines the separation channel. Typical macro systems have a length of 30–60 cm, a thickness of no less than 150  $\mu$ m and a width of about 2 cm. As mentioned previously, the resolution is inversely proportional to the height of the channel when all other parameters are kept constant. Micromachining can be used to increase the resolution by decreasing channel thickness to as small as 10  $\mu$ m (possibly even smaller). Additionally, the ability to precisely define the channel and electrodes improves resolution by reducing band broadening [1].

Several prototype  $\mu$ -EFFF systems have been fabricated using micromachining technologies as outlined in Fig. 5 [38]. Using 3-in (76 mm)  $\langle 100 \rangle$  single-side polished silicon wafers, we deposited 2500 Å of Si<sub>3</sub>N<sub>4</sub> with a plasma enhanced-chemical vapor deposition (PE-CVD) device. The Si<sub>3</sub>N<sub>4</sub> was then patterned using photoresist as a mask on both sides of the wafer in preparation for KOH etching. 1-mm-square openings were made in the Si<sub>3</sub>N<sub>4</sub> on the unpolished side of the wafer in a CF<sub>4</sub> plasma. Bulk anisotropic etching in a 20% KOH solution at 56 °C for 24 h [39] was then used to define the input and output ports as demonstrated in Fig. 5(a). The KOH etching process left a thin Si<sub>3</sub>N<sub>4</sub> membrane about 1000- to 2000-Å thick on the front side of the wafer. Accounting for the sidewall profile of the etch, the openings on the polished side of the wafer were about 400- $\mu$ m square. 1000 Å of titanium followed by 1500 Å of gold were sputtered on the polished side of the wafer. The metals were patterned to form the channel electrodes using a photoresist mask and a mixture of 400-g KI, 100-g I<sub>2</sub>, and 400-mL H<sub>2</sub>O (Iodine etch) to etch the gold and a 1% hydrofluoric acid (HF) solution to etch the titanium as shown in Fig. 5(b). Thick photosensitive polyimide micro molding (using Amoco Ultradel 7505) was used to define the micro-flow channels (10–40  $\mu$ m in height) as indicated in Fig. 5(c) [29]. The polyimide was spun on to the wafers and then placed on a leveling plate for 15 min to ensure an even coat and eliminate any potential thickness irregularities. After UV patterning and development, the photosensitive polyimide was completely cured in an oven at 350 °C for 6 h. The thin Si<sub>3</sub>N<sub>4</sub> membrane was then removed using a CF<sub>4</sub> reactive ion etch (RIE) [see Fig. 5(d)]. 1000 Å of titanium and 1500 Å of gold were then sputtered on the unpolished side of the wafer [see Fig. 5(e)]. Because of the presence of the etched input and output ports, there was now an electrical connection between the front side electrodes and the backside of the wafer. These electric feedthroughs made it possible to make good contact with the front side electrodes. 1000 Å of titanium and 1500 Å of gold were then sputtered on a glass substrate that had been cut to fit over a group of  $\mu$ -EFFF channels [Fig. 5(f)]. The titanium and gold were subsequently patterned to form the second electrode using the same titanium and gold etches mentioned previously. This top electrode must be patterned such that it can be contacted during operation of the system. Care must be taken during the patterning process to place photoresist on the sidewall of the glass substrate at the point

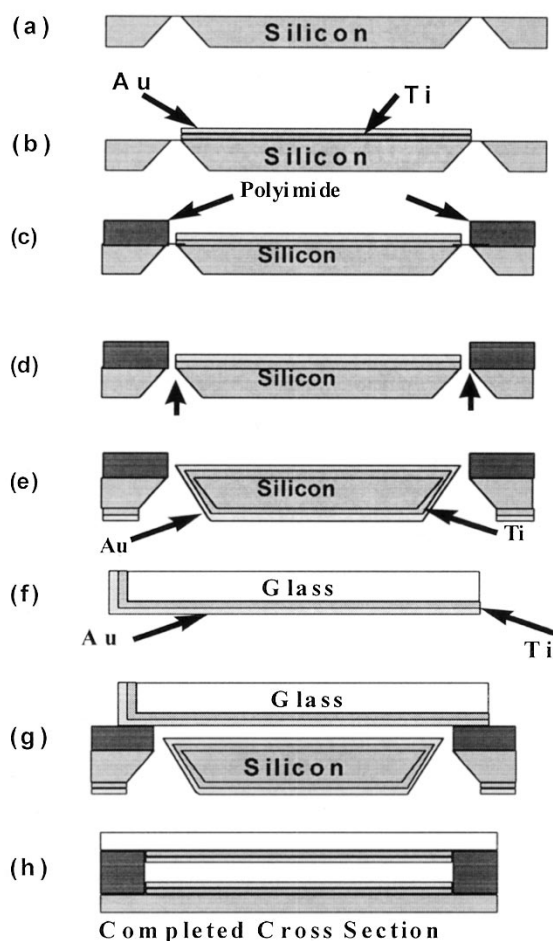


Fig. 5. Process flow diagram for the  $\mu$ -EFFF system. (a) Etching of input and output ports in silicon. (b) Deposition and patterning of titanium and gold electrode. (c) Application and patterning of polyimide. (d) Removal of  $\text{Si}_3\text{N}_4$  membranes. (e) Deposition of backside titanium and gold electrodes. (f) Deposition and patterning of titanium and gold on glass substrate. (g) Bonding of glass and silicon substrate. (h) Cross section of completed  $\mu$ -EFFF system.

where the electrode reaches the edge. The glass and silicon substrates were finally bonded together using a UV curable, biocompatible adhesive (3341 Medical Device Adhesive from Loctite, Hartford, CT) [Fig. 5(g)]. The glass substrate was pressed against the silicon substrate with the electrodes aligned while the UV adhesive was dispensed near the polyimide-glass interface and allowed to flow between the substrates due to capillary action. Once the adhesive had completely surrounded the channel, it was cured using a UV lamp. A cross section at this point is shown in Fig. 5(h). A conductive adhesive was used to bond a wire to the contact pad on the glass substrate allowing a lead to be easily attached. Steel tubing with an inner diameter of  $125\ \mu\text{m}$  was attached to the silicon substrate over the input and output ports using a ferrule bonded to the silicon substrate. The  $\mu$ -EFFF devices created using this process are 4 and 6 cm in length with aspect ratios between 20–400.

It should be noted that the micromachined  $\mu$ -EFFF systems are only part of a larger analysis system that includes a pump, flow-rate controller, detector, recorder, and fraction collector. A schematic of the connections for these parts is shown in Fig. 6.

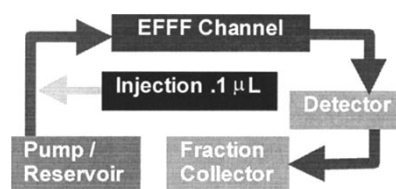


Fig. 6. Schematic of entire EFFF analysis system showing the fluid and electrical connections as well as other components required for system operation.

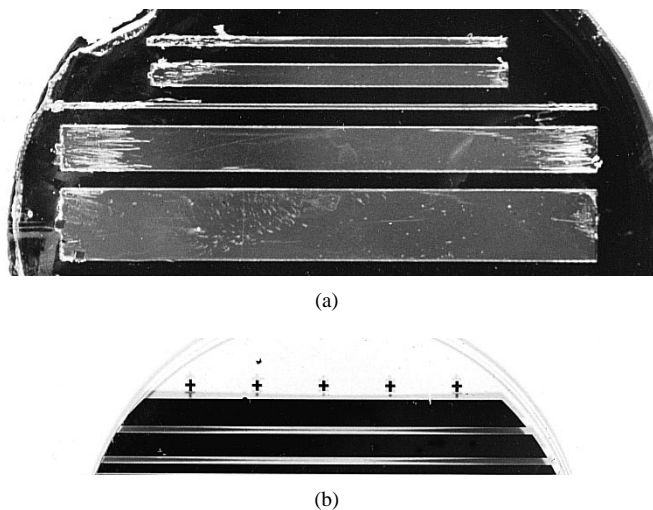


Fig. 7. (a) Photograph of silicon substrate with patterned titanium and gold electrodes and patterned polyimide channels. (b) Photograph of glass substrate with patterned titanium and gold electrodes.

In order to perform separations using the  $\mu$ -EFFF devices, one entrance of a T connector is attached to the steel tubing while another entrance is covered with a septum for sample injection. The sample is injected through the septum and into the T using a  $10\text{-}\mu\text{L}$  Hamilton syringe containing the sample plug. The other opening on the T connector is linked to a syringe pump using 10 cm of Teflon tubing with a 0.8-mm outer diameter and a  $350\text{-}\mu\text{m}$  inner diameter. The output port is connected to a linear UV-106 absorbance detector (monitoring extinction at 254 nm) using 3 cm of  $350\text{-}\mu\text{m}$  inner diameter Teflon tubing. The fluid output from the detector can be connected to a fraction collector if desired. The detector is electrically connected to a recording device (either a PC or strip chart recorder) which collects the data output from the detector as well as the measured current and the applied voltage. The power to the top and bottom electrodes is provided by an Hewlett Packard 6128C DC power supply.

## V. RESULTS

A number of  $\mu$ -EFFF channels have been fabricated with a wide range of dimensions. The channel thickness ranges between 20–30  $\mu\text{m}$ , the lengths vary from 4–6 cm and the channel widths are from 0.4–8 mm. A picture of the silicon substrate with polyimide channels and the Au/Ti electrodes is shown in Fig. 7(a). A picture of the glass substrate with the patterned Au/Ti electrodes is shown in Fig. 7(b).

TABLE I  
RESULTS OF POLYIMIDE (AMOCO ULTRADEL 7505) SWELLING TESTS IN DI WATER

Uncured ( $\mu\text{m}$ )	Cured ( $\mu\text{m}$ )	Shrinkage	Soaked in $\text{H}_2\text{O}$ ( $\mu\text{m}$ )	Swelling
9.1	5.0	45%	5.0	0%
16.3	11.5	30%	11.9	3.0%
27.5	15.5	44%	15.9	2.9%
57	28.0	51%	28.4	1.4%
60	29.0	52%	30.0	3.4%
66	34.5	48%	35.3	2.3%
Average	—	45%	—	2.2%

TABLE II  
RESULTS OF HEMOLYSIS TESTING ON THE MATERIALS  
USED TO FABRICATE THE  $\mu$ -EFFF SYSTEM

Sample	Absorbance	% Hemolysis
Detergent (+ Control)	1.35	100
Glass (– Control)	.025	0
Grushed $\mu$ -EFFF devices	.025	0
Polyimide	.01	0
Silicone Rubber	.04	1.14

The channels have been tested for mechanical integrity by forcing flows with velocities as high as 4 cm/s through the channels and checking for leaks (normal operating flows are typically 1 cm/s and lower).

The amount of potential polyimide swelling was found by spinning the photosensitive polyimide on six wafers at a series of thicknesses (estimated), patterning the polyimide in the same manner as for the  $\mu$ -EFFF devices, curing the polyimide for 24 h at 285 °C, and then soaking the polyimide in deionized (DI) water for 24 h at room temperature. The results of these tests are shown in Table I. Examination of Table I reveals that polyimide swelling in water is potentially significant. Since the channel thickness is of critical importance in  $\mu$ -EFFF systems, a variation in channel thickness can have a ripple effect through the system and cause results that vary from the expected. The 2.2% swelling measured is small enough, though, to not cause significant differences, especially when considering that the amount of swelling in the actual devices will be much less. Only the polyimide that makes up the sidewalls of the channel will be exposed to the buffer solution in the  $\mu$ -EFFF devices; its height is typically on the order of 20  $\mu\text{m}$ . Thus, a much smaller surface area will be exposed to the buffer solution in practice than in these tests. In addition, the glass substrate bonded to the top side of the polyimide is bonded in areas far from the location of the buffer solution and will likely prevent any significant swelling in the areas close to the buffer solution. Thus, swelling of the polyimide is unlikely to significantly affect the operation of the  $\mu$ -EFFF devices.

The results of the hemolysis tests are shown in Table II. Examining these results, we concluded that very little, if any, hemolysis had taken place, since the measured absorbance for all samples of interest was very close to the negative control. Therefore, it appears that the materials chosen are reasonable for use in separating cells and cellular components, at least in the area of cell lysis.

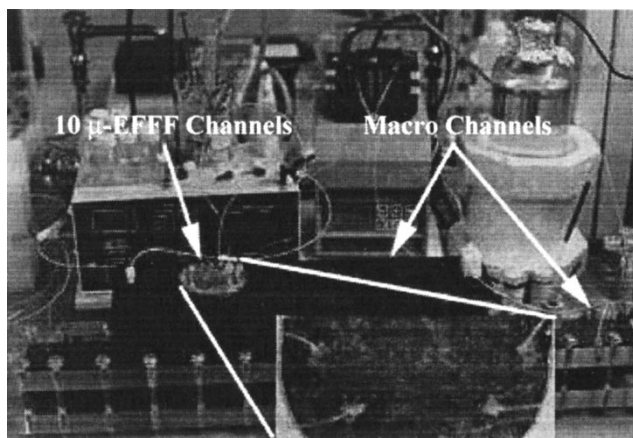


Fig. 8. Photograph of both a  $\mu$ -EFFF system and a previous generations of macro EFFF systems.

Fig. 8 shows a photograph of the  $\mu$ -EFFF system and two macro-scale EFFF systems for comparison along with some of the pump and detector equipment used. The macro EFFF systems are both single-channel systems, one with a length of 64 cm and the other with a length of 30 cm and both are similar to systems now in the midst of commercial development. There are ten  $\mu$ -EFFF devices on the wafer pictured. Notice that the  $\mu$ -EFFF devices are less than 0.5 cm in overall thickness while the macro channels are well over 10-cm thick.

The electrical connections have been tested by measuring the resistance through the system. The resistance of the electrode system connecting the front to the back (through the input and output ports) of silicon wafer is less than 5  $\Omega$ . The resistance in connecting to the front side of the glass substrate is also less than 5  $\Omega$ . The measured resistance across channel 1 with a 20- $\mu\text{M}$  solution filling the channel is about 40 k $\Omega$ , which at 1.7 V yields currents of about 42  $\mu\text{A}$ . These numbers for current and voltage confirm the theoretical prediction that Joule heating would not be a concern in the system since the maximum expected temperature change is less than 1 °C using these numbers with flow rates as low as 0.01 cm/s. As will be discussed, these measured currents are somewhat lower than expected, but even with increased currents Joule heating appears insignificant.

To perform the plate height calculations 100 nL samples of acetone were injected into the system for a series of flow rates. The plate height calculations were done using the equations given previously and the results were plotted to determine the instrumental component of the plate height.

The results of the plate height calculations for the  $\mu$ -EFFF system are shown in Fig. 9. For comparison, the results are shown with typical plate height calculations for current macro FFF systems and an earlier reported micromachined system from our lab [38]. As can be seen in the graph, the measured instrumental plate height for the  $\mu$ -EFFF system is very close to that of the best macro systems, about 400  $\mu\text{m}$ . Theoretically, the band broadening of the  $\mu$ -EFFF system should be much smaller than that of the other systems for all ranges of flow velocities. The fact that it is not at the lowest flow velocities indicates that the band broadening due to the instrument (i.e., connections between the channels, injection system, and

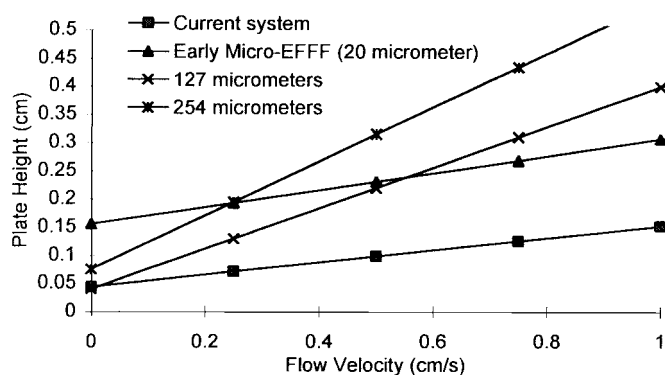


Fig. 9. Measured plate heights for the current  $\mu$ -EFFF channel, an earlier reported  $\mu$ -EFFF system, a 254- $\mu$  EFFF channel, and a 127- $\mu$  EFFF channel.

detector) needs to be reduced. The slope of the plate height line is largely influenced by the thickness of the channel. Thus, the band broadening seen in the  $\mu$ -EFFF channel at higher flow rates is lower than for the larger channels. These plate height results may also be caused by difficulty in producing a small sample volume. Scaling from macro systems, the sample volume should be on the order of 50 nL while our typical samples volumes are no smaller than 100 nL. Work is continuing in both of these areas. Potential improvement may also be found if a less concentrated sample is used, but this approach reduces detectability.

The results of the acetone runs used to perform the band-broadening calculations allowed us to also calculate the dead volume in the system. The dead volume is the volume of the tubes, connectors, and injection system that are not directly a part of the  $\mu$ -EFFF channels. This dead volume causes delay in the transport of buffer and the injected sample from the injection point to the channel and from the channel to the detector. This delay must be accounted for if the mathematical model of the EFFF system is to be applied accurately. The dead volume was estimated to be about 13.8  $\mu$ L. At a volume flow rate of 1 mL/h (0.174 cm/s in the channel) this causes a delay of about 50 s in our channel. Again these values indicate that the connections between the micro and macro worlds need to be improved.

Separations are performed in the  $\mu$ -EFFF system by injecting samples as small as 100 nL into the system while the flow is on. After a few seconds (depending on the flow velocity in use to allow the sample to just enter the  $\mu$ -EFFF channel) the flow is stopped for a short time (less than 10 s) to allow the sample in the channel to equilibrate. The flow is again started and the separation is then performed. The voltage and current are continuously monitored during the separation to ensure that consistent fields are found in the channel.

A typical separation run through the  $\mu$ -EFFF system is shown in Fig. 10. This run was performed using a 0.1- $\mu$ L mixture of 44, 130, and 261 nm polystyrene particles (from Bangs Laboratories, Fishers, IN) and had an applied voltage of 1.9 V, a current of 165  $\mu$ A, a flow velocity of 0.08 cm/s, a buffer of DI water, a channel length of 6 cm, and a channel thickness of 28  $\mu$ m. A 10-s relaxation period was used after allowing 30 s for the sample plug to reach the  $\mu$ -EFFF channel. Note that all of the particles are clearly separated

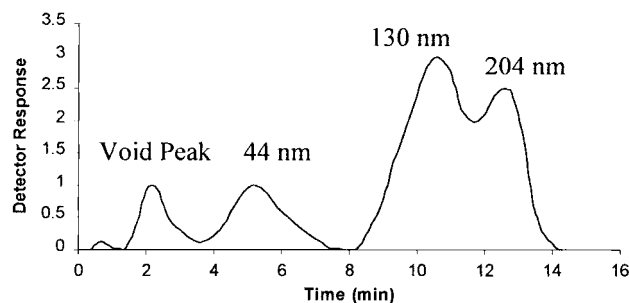


Fig. 10. Example of a separation performed in  $\mu$ -EFFF system. The separation was performed by injecting a 0.1- $\mu$ L mixture of 44-, 130-, and 261-nm polystyrene particles into a 28- $\mu$ m channel with an applied voltage of 1.9 V, a current of 165  $\mu$ A, a flow velocity of 0.08 cm/s, a DI water buffer, and a channel length of 6 cm.

TABLE III  
COMPARISON OF THE DIMENSIONS AND PERFORMANCE  
OF THE  $\mu$ -EFFF SYSTEM WITH MACRO EFFF SYSTEMS

Parameter	Macro	$\mu$ -EFFF
Channel Length	37 cm	4-6 cm
Channel Thickness	127 $\mu$ m	20-30 $\mu$ m
Aspect Ratio	100	Up to 400
Relaxation Time	45 s	1.5 s
Measured Number of Plates	925	150
Theoretical Plates	31 000	31 200
Sample Size	5 $\mu$ L	0.1 $\mu$ L
Parallel Channels	None	10
Run Times	60 min	15min
Field Strengths with 1.7 V	95 V/cm	850 V/cm

from the void peak and from each other. A resolution similar to this in the current macro systems would take about 1 h to accomplish. While the resolution between the 130- and 204-nm particles is not high, the separation parameters were not ideal for separating these particles from each other and the resolution can be improved for separations in this size range. Using a curve fit of previously collected data from macro EFFF systems to estimate the effective field in the channel at this current, the predicted elution time using (3) and (4) is 3.0 min for the 44-nm particles, 8.1 min for the 130-nm particles, and 12.5 min for the 204-nm particles. If the void time of 65 s and the delay time at this flow rate of 80 s is taken into account, the results obtained are in fairly good agreement with theory. The 44-nm particles elute slightly later than expected, while the 204-nm particles are somewhat early. This variation during the run may be explained by a slowing dropping current (and by association the effective voltage) in the channel as the run progresses. Our setup does not insure a constant current and our measured current for the run is an average for the run. Additionally, little is known about how the effective voltage will vary in the channel as compared to macro systems. The measured effective voltage for this run is only 0.5% of the applied voltage which is somewhat lower than that for macro systems. This effect will be further examined in future communications.

Table III gives a comparison of the parameters for typical macro EFFF systems compared to the  $\mu$ -EFFF system demonstrated here. Note the great improvements in system

size, aspect ratio, relaxation time, sample size, run times, and parallel operation. The reduction in system size should allow for the possibility of portable EFFF systems and a decrease in the laboratory space required for the current systems. The increased aspect ratio should lessen the impact of edge effects in the system and thereby reduce plate heights. The reduction in relaxation times and run times should speed analysis in the laboratory. The reduction in sample sizes alleviates the need to greatly multiply a sample before analysis (as is done in DNA amplification by PCR) or to reduce the effort needed to collect a sample large enough for analysis. The parallel channels allow for multiple tests to be run at the same time. The batch fabrication methods inherent in micromachining technologies will also allow for the design of disposable systems eliminating the need for cleaning the systems after every use. By improving the macro/micro interfaces, implementing an on-chip detection system, and reducing sample sizes even further, the  $\mu$ -EFFF systems will become even more powerful, faster, and reliable as a chemical and biological analysis tool.

## VI. CONCLUSION

In this work, micromachining technologies were used in the development of the next generation of precision  $\mu$ -EFFF separation systems. Micromachining technologies were used to overcome some of the difficulties associated with macro-scale EFFF systems. EFFF systems have several advantages when compared to other separation systems including a gentle separation field that allows for separation of delicate particles, and a separation field perpendicular to the flow direction which reduces the reliance of resolution on field strength. EFFF theory predicts that a reduction in channel height will improve the resolution. This theory was demonstrated using the  $\mu$ -EFFF system. A method of fabrication using micromachining technologies for  $\mu$ -EFFF system construction was described. The  $\mu$ -EFFF system was tested and compared favorably to the current macro EFFF systems, especially in the areas of separation times and sample volumes. By further improving the design, interfaces, and assembly of the  $\mu$ -EFFF devices demonstrated in this paper, a powerful new system for chemical and biological analysis will be realized.

## REFERENCES

- [1] K. D. Caldwell, "FFF of biological materials," in *Research Instrumentation for the 21st Century*, G. Beecher, Ed. Dordrecht, The Netherlands: Martinus Nijhoff, 1987, pp. 89–116.
- [2] M. C. Roman and P. R. Brown, "Free-flow electrophoresis as a preparative separation technique," *Anal. Chem.*, vol. 66, pp. 86A–94A, Jan. 15, 1994.
- [3] K. D. Caldwell, L. F. Kesner, M. N. Meyers, and J. C. Giddings, "Electrical field-flow fractionation of proteins," *Science*, vol. 176, pp. 296–298, 1972.
- [4] C. S. Effenhauser, A. Manz, and M. H. Widmer, "Glass chips for high-speed capillary electrophoresis separations with submicrometer plate heights," *Anal. Chem.*, vol. 65, pp. 2637–2642, 1993.
- [5] C. S. Effenhauser, A. Paulus, and A. Manz, "High-speed separation of antisense oligonucleotides on a micromachined capillary electrophoresis device," *Anal. Chem.*, vol. 66, pp. 2949–2953, 1994.
- [6] S. C. Jacobson, A. W. Moore, and J. M. Ramsey, "Fused quartz substrates for microchip electrophoresis," *Anal. Chem.*, vol. 67, pp. 2059–2063, 1995.
- [7] A. T. Woolley and R. A. Mathies, "Ultra-high-speed DNA sequencing using capillary electrophoresis chips," *Anal. Chem.*, vol. 67, pp. 3676–3680, 1995.
- [8] D. E. Raymond, A. Manz, and H. M. Widmer, "Continuous sample pretreatment using a free-flow electrophoresis device integrated onto a silicon chip," *Anal. Chem.*, vol. 66, pp. 2858–2865, 1994.
- [9] ———, "Continuous separation of high molecular weight compounds using a microliter volume free-flow electrophoresis microstructure," *Anal. Chem.*, vol. 68, pp. 2515–2522, 1996.
- [10] G. Ocvirik, E. Verpoorte, A. Manz, and H. M. Widmer, "Integration of a micro liquid chromatograph on to a silicon chip," in *Proc. Transducers'95*, p. 191.
- [11] S. C. Terry, J. H. Jerman, and J. B. Angell, "Gas-chromatographic air analyzer fabricated on silicon wafer," *IEEE Trans. Electron. Devices*, vol. ED-26, pp. 1880–1886, 1979.
- [12] S. J. Doherty and W. L. Winniford, "Rapid on-line analysis using a micromachined gas chromatograph coupled to a bench-top quadrupole mass spectrometer," *LC-GC*, vol. 12, pp. 846–850, 1994.
- [13] R. A. Mowery, "Determining the calorific value of natural gas using a silicon micromachined process gas chromatographic analyzer," *ISA Trans.*, vol. 25, pp. 1–9, 1986.
- [14] A. W. Moore, S. C. Jacobson, and J. M. Ramsey, "Microchip separations of neutral species via micellar electrokinetic capillary chromatography," *Anal. Chem.*, vol. 67, pp. 4184–4189, 1995.
- [15] J. C. Giddings, "Non-equilibrium theory of field-flow fractionation," *J. Chem. Phys.*, vol. 49, pp. 81–85, July 1, 1968.
- [16] ———, "Parameters for optimum separations in field-flow fractionation," *Sep. Sci.*, vol. 8, pp. 567–575, 1973.
- [17] ———, "Field-flow fractionation: Extending the range of liquid chromatography to one trillion ( $10^{12}$ )," *J. Chromatogr.*, vol. 125, pp. 3–16, 1976.
- [18] J. C. Giddings and K. D. Caldwell, "Field flow fractionation," in *Physical Methods of Chemistry*, vol. IIIB, B. W. Rossiter and J. F. Hamilton, Eds. New York: Wiley, 1989.
- [19] J. C. Giddings and M. R. Schure, "Theoretical analysis of edge effects in field-flow fractionation," *Chem. Eng. Sci.*, vol. 42, pp. 1471–1479, 1987.
- [20] M. E. Hovsing, G. H. Thompson, and J. C. Giddings, "Column parameters in thermal field-flow fractionation," *Anal. Chem.*, vol. 42, pp. 195–203, Feb. 1970.
- [21] A. S. Said, *Theory and Mathematics of Chromatography*. Heidelberg, Germany: Huethig, 1981.
- [22] K. D. Caldwell and Y. S. Gao, "Electrical field-flow fractionation in particle separation. Monodisperse standards," *Anal. Chem.*, vol. 65, pp. 1764–1772, July 1, 1993.
- [23] P. H. Wiersema, A. L. Loeb, and J. T. G. Overbeek, "Electrophoretic mobility of a spherical colloidal particle," *J. Colloid Interface Sci.*, vol. 22, pp. 78–99, 1966.
- [24] R. W. O'Brien and L. R. White, "Electrophoretic mobility of a spherical colloidal particle," *J. Chem. Soc. Faraday Trans. 2*, vol. 74, pp. 1607–1626, 1978.
- [25] X. N. Jiang, Z. Y. Zhou, J. Yao, Y. Li, and X. Y. Ye, "Microfluid flow in microchannel," in *Proc. Transducers'95*, pp. 317–320.
- [26] J. P. Brody and P. Yager, "Low reynolds number micro-fluidic devices," in *Proc. Solid-State Sensors and Actuator Workshop*, 1996, pp. 105–108.
- [27] A. C. Hoogerwerf and K. D. Wise, "A three-dimensional microelectrode array for chronic neural recording," *IEEE Trans. Biomed. Eng.*, vol. 41, pp. 1138–1146, 1994.
- [28] D. S. Soane, *Polymers in Microelectronics*. New York: Elsevier, 1989, pp. 15–211.
- [29] A. B. Frazier and M. G. Allen, "Metallic microstructures fabricated using photosensitive polyimide electroplating molds," *J. Microelectromech. Syst.*, vol. 2, pp. 87–94, 1993.
- [30] G. Peluso, O. Petillo, L. Ambrosio, and L. Nicolais, "Polyetherimide as biomaterial: Preliminary *in vitro* and *in vivo* biocompatibility testing," *J. Mat. Sci.: Materials in Medicine*, vol. 5, pp. 738–742, 1994.
- [31] T. G. H. Yuen and W. F. Agnew, "Histological evaluation of polyesterimide-insulated gold wires in brain," *Biomat.*, vol. 16, pp. 951–956, 1995.
- [32] E. Csoregi, D. Schmidtke, and A. Heller, "Design and optimization of a selective subcutaneously implantable glucose electrode based on wired glucose oxidase," *Anal. Chem.*, vol. 67, pp. 1240–1244, Apr. 1, 1995.
- [33] D. L. Wang and A. Heller, "Miniaturized flexible amperometric lactate probe," *Anal. Chem.*, vol. 65, pp. 1069–1073, Apr. 15, 1993.
- [34] R. R. Richardson, J. A. Miller, and W. M. Reichert, "Polyimides as biomaterials: Preliminary biocompatibility testing," *Biomat.*, vol. 14, pp. 627–635, 1993.
- [35] J. B. Park and R. Lakes, *Biomaterials: An Introduction*, 2nd ed. New York: Plenum, 1992.

- [36] J. Black, *Biological Performance of Materials: Fundamentals of Biocompatibility*, 2nd ed. New York: Marcel-Dekker, 1992.
- [37] X. M. Tong and K. D. Caldwell, "Separation and characterization of red blood cells with different membrane deformability using steric field-flow fractionation," *J. Chromatogr. B: Biomed. Appl.*, vol. 674, pp. 39–47, 1995.
- [38] B. K. Gale, A. B. Frazier, and K. D. Caldwell, "Micromachined electrical field-flow fractionation system," in *Proc. MEMS'97*, pp. 119–124.
- [39] H. Siedel, L. Csepregi, and A. Heuberger, "Anisotropic etching of crystalline silicon in alkaline solutions," *J. Electrochem. Soc.*, vol. 37, pp. 3612–3620, 1990.



**Bruce K. Gale** (S'98) is a Ph.D. degree candidate in his third year of study in the Department of Bioengineering at the University of Utah, Salt Lake City. His work is funded by a National Science Foundation Graduate Fellowship.

Mr. Gale received the B.S. degree in mechanical engineering from Brigham Young University in 1995. His interests include medical and biological based applications of micromachining and his work has recently involved micromachined particle separation systems and detectors.



**Karin D. Caldwell** received the B.S. degree in organic chemistry from the University of Uppsala, Uppsala, Sweden, in 1964. Her subsequent degrees of Fil.Lic. (Ph.D., 1968) and Fil. Dr. (Dr.Sci., 1976), both in biochemistry, were from the same institution.

Her research has centered on the development of methodology for separation and characterization of biochemical samples. Of specific interest is the use of the field-flow fractionation techniques to analyze degrees of surface modification of model colloids.



**A. Bruno Frazier** (S'85–M'85) received the B.S. and M.S. degrees in electrical engineering from Auburn University, Auburn, AL, in 1986 and 1987, respectively. In December 1993, he received the Ph.D. degree in electrical engineering from Georgia Institute of Technology. From 1990–1993, he attended Georgia Institute of Technology, Atlanta, and conducted research into micromachining processes for the fabrication of metallic microstructures, development and characterization of micromachining materials, as well as micromachined devices utiliz-

ing the previously developed processes and materials.

From 1987–1990, he worked for Intergraph Corporation, Huntsville, AL, in the development of computer-aided graphics systems. After graduating, he conducted research in micromachining technologies at the University of Michigan, Ann Arbor, as a Visiting Scholar through June 1995. In August 1995, he joined the bioengineering and electrical engineering faculty at the University of Utah, Salt Lake City. His current research interests include optical, magnetic, and biomedical applications of micromachining technology.

Dr. Frazier was awarded the ISHM Educational Fellowship two consecutive terms during his graduate studies.